Ocean Engineering 285 (2023) 115421

Contents lists available at ScienceDirect

Ocean Engineering

journal homepage: www.elsevier.com/locate/oceaneng

Centrifuge testing of improved monopile foundation for offshore wind turbines

Yazeed A. Alsharedah [a,*], Jonathan A. Black [b], Timothy Newson [c], M.H. El Naggar [c]

[a] Department of Civil Engineering, Qassim University, Saudi Arabia
[b] Department of Civil Engineering, Queen University of Belfast, Northern Ireland, United Kingdom
[c] Department of Civil & Environmental Engineering, Western University, Canada

ARTICLE INFO

Handling Editor: A.I. Incecik

Keywords:
Offshore wind farms
Monopile
Hybrid foundation
Cyclic lateral loading
Clay

ABSTRACT

Large fixed vertical offshore wind turbine (OWT) tower structures are typically used to transfer complex loads to the foundations from a combination of wind, waves, and self-weight. These loads must be accommodated within a very small rotation envelope and natural frequency bands to allow the turbines to operate effectively. These challenging loading conditions and strict operational requirements can lead to extremely costly foundation designs. Several foundation options are available to support these turbines, with monopiles currently accounting for 80% of the installed capacity with routinely used diameters of 5–8 m and depths of penetration of 30–80 m. To limit monopile diameters and penetration depths, an improved monopile design: the 'hybrid foundation' comprising a plate and centrally located pile, is proposed as an alternative to monopiles. A series of scaled physical model centrifuge tests were conducted to investigate the benefits of the hybrid foundation system and compare its behavior with the typically used monopiles. This type of foundation system can enhance the performance of an OWT since the turbines are subjected to high lateral loads and overturning moments. Centrifuge modeling has been used to investigate the lateral capacity and stiffness of the foundations under lateral monotonic and cyclic loading conditions. Two models were tested: a standard monopile (MP) and a hybrid foundation (HF). Lateral loads were applied with eccentricity for both models to replicate prototype (field) conditions. Models were tested at 50g in over-consolidated clay beds. These soil samples were prepared using inflight consolidation and subjected to a sand surcharge, to increase the shear strength in the zone of influence of the model foundations. Monotonic lateral loading results indicated that the addition of a plate improves the relative lateral ultimate capacity, whilst enabling a reduction of monopile penetration depth and diameter for similar capacities. Specifically, similar capacity/stiffness was realized for the HF system compared to the MP. One-way cyclic lateral loading indicated both the HF and the MP had a shakedown response under fatigue loading of up to 10000 cycles, which indicates the potential use of this novel system for future developments.

1. Introduction

Our world is moving towards less dependence on fossil fuels driven by many factors such as global warming, sustainability, and geopolitics. Alternatives, therefore, must be clean, reproducible, and economically viable. Alternatives include biomass/nuclear-powered plants, solar energy, hydropower, and wind energy. Of these, wind energy plays an important role in global sustainable/cost-efficient electricity power production. Multiple groups of turbines are typically used to form wind farms that are installed onshore or offshore. Recently, many offshore wind farms (OWF) were constructed around the world due to space availability and aesthetic problems associated with their onshore counterparts. These OWFs generally have large footprints and experience longer uninterrupted periods of wind compared with their onshore counterparts, hence typically providing higher power production (Lombardi et al., 2013). However, this comes at a penalty of higher grid costs, difficulty in maintenance, and, from a civil engineering perspective, more complicated loading as a result of combined waves and wind actions leading to relatively costly foundation options.

Typically, OWF support structures are fixed to the seabed, with floating systems still in the research realm. Most of these fixed structures (about 80%) are founded on monopiles (MP) with routinely large

* Corresponding author.
E-mail addresses: y.alsharredah@qu.edu.sa (Y.A. Alsharedah), j.black@qub.ac.uk (J.A. Black), tnewson@eng.uwo.ca (T. Newson), naggar@uwo.ca (M.H. El Naggar).

https://doi.org/10.1016/j.oceaneng.2023.115421
Received 8 January 2023; Received in revised form 10 July 2023; Accepted 17 July 2023
Available online 29 July 2023
0029-8018/

diameters of 5–8m. Other types of fixed support include gravity base foundations (GBF), jacket steel structures, and suction caissons (Abdelkader, 2016; Byrne and Houlsby, 2003). The turbine is carried on a tapered tower (superstructure), which is 3–6 m in diameter at its base, that is supported on a transition piece that mounts on the foundation system (substructure). The tower diameter must be designed to withstand vertical and lateral loads and have sufficient capacity against buckling, whilst being small enough to prevent increased wave, current and wind loadings. The foundation, on the other hand, must be designed carefully to absorb all of the loads from the superstructure and also meet the serviceability limit state. A variety of loads act upon the turbine components from waves, wind, tides, currents, ice, rotor frequency (1P), and blade passing frequency (3P) loadings. These loads, which are predominantly cyclic in nature, are transferred from the tower to the foundation and the seabed leading to displacement and rotation, and fatigue.

Besides the ultimate limit state two issues are also important when designing a substructure for an offshore wind turbine (OWT):

1) The structure's natural frequency and its variation with repeated loading during the operational service period (typically 2–30 years)
2) Permissible rotation of the foundation, which is typically less than 0.5° (Malhotra, 2009)

With increased capacity and strict rotation requirements coupled with increased developments in deeper water to harness more wind power, it is anticipated that monopile diameters will continue to increase, posing problems of drivability and cost for the development of new OWFs. Hence, researchers have been proposing alternative foundation forms to address these issues. One of these is the novel hybrid foundation (HF) system comprising a circular plate fitted with a smaller and shorter monopile. In this paper, we investigate and compare this novel foundation system to a monopile (MP) using centrifuge testing to establish the following:

1. The different behaviors of the MP and HF foundation systems under laterally applied monotonic and cyclic loading by using scaled models;
2. Damage accumulation relationships describing the foundation angular rotation as a function of loading characteristics and the number of cycles for these systems;
3. The calibration/validation of FEM models using 1 and 2 above for further research.

Several researchers have attempted to use hybrid foundation systems previously, which is a plate fitted with a short monopole in its center, intending to reduce the monopole diameter in both sands and clays (Stone et al., 2007; El-Marassi et al., 2008). The HF is believed to have improved lateral load response over MP through the restoring moment due to its plate weight, the absorbed shear stresses through its plate contact with soil, the increased passive pressure against the pile face, and the restoring moment from the soil contact pressure (Lehane et al., 2014).

Using centrifuge modelling, Powrie and Daly (2007) studied an embedded retaining wall with a stabilizing base in kaolin clay. Their results indicated the beneficial effects of the stabilizing base on the retaining wall system. Wang et al. (2018) conducted a centrifuge study to investigate different OWT foundation systems, including a monopile, a gravity base, and two hybrid foundations installed in a sand deposit and subjected to laterally applied monotonic and cyclic loading. They concluded that hybrid foundation systems had higher stiffness compared to monopile for resisting lateral loads. Lehane et al. (2014) investigated the lateral and rocking responses of different hybrid foundations and suggested that the hybrid foundation plate improves foundation performance compared to monopiles. Cherchia (2016) suggested that hybrid foundations can have a considerable cost advantage because the

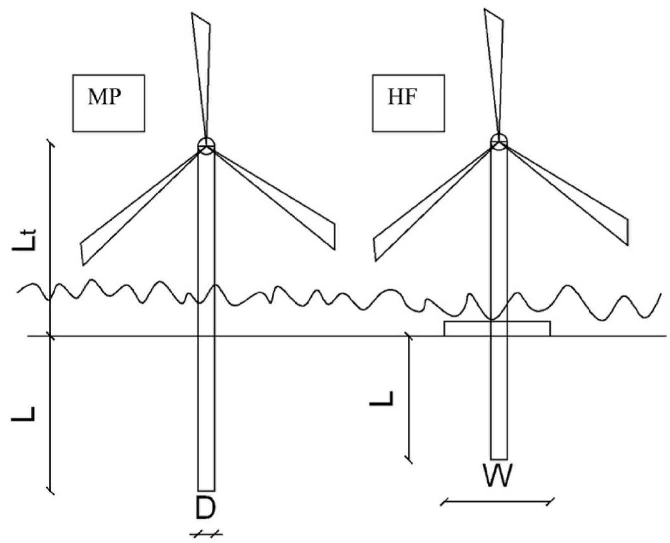

Fig. 1. Model foundations cross section and geometric definitions.

diameter and length of their pile are reduced compared to a monopile counterpart, and the material weight could be significantly lower than that of a monopile. However, few studies exist on the cyclic performance of the OWTs and their long-term response to cyclic loading and the progressive increase of rotation during their lifetime. Hence this paper aims to close this gap in the literature. This paper describes the investigation of monotonic and cyclic lateral loading tests on model foundations of a monopile and a hybrid foundation installed in an over-consolidated kaolin clay. The results from this study may support future applications of this novel foundation system.

2. Centrifuge modelling

The centrifuge testing program was conducted at the Centre of Energy and Infrastructure Ground Research (CEIGR) at the University of Sheffield, UK. The 4 m diameter beam centrifuge had a payload of 50 g t and is equipped with a 32-channel National Data Acquisition System (Black et al., 2014). All models were tested at 50g. To increase the efficiency of the tests and reduce preparation time, multiple tests were conducted within a single centrifuge box. The headwork was designed to be movable, which facilitated maneuverability from test to test. Test locations were maintained at 7 diameters center to center, while the loading direction was always towards the box centreline, to avoid the effects of the rigid boundaries.

2.1. Objectives of the centrifuge program

Two foundation options were investigated and compared to each other in an over-consolidated kaolin clay, namely, a monopile (MP) of length to diameter (L/D) ratio of 4.4 and prototype pile length of 7.26 m and diameter of 1.65 m and a hybrid foundation (HF) with prototype plate diameter (W) of 2.5 m, pile diameter (D) of 1.1 m and length of penetration (L) of 5 m. Fig. 1 shows the two considered systems.

The Speswhite kaolin clay used was made by Imerys, UK. The testing program included two series of tests including four monopile tests and four hybrid foundation tests. In the first series, two undrained monotonic loading probes were conducted to obtain the monopile lateral ultimate capacity, H_u, and to confirm the repeatability of tests. This was followed by two cyclic loading tests to establish the behavior of the monopile under laterally applied cyclic loading. In the first cyclic loading test, the fatigue limit state was considered, and the monopile underwent one-way cyclic lateral loading for 11000 cycles. This was followed by a second cyclic lateral loading test in which one-way cyclic

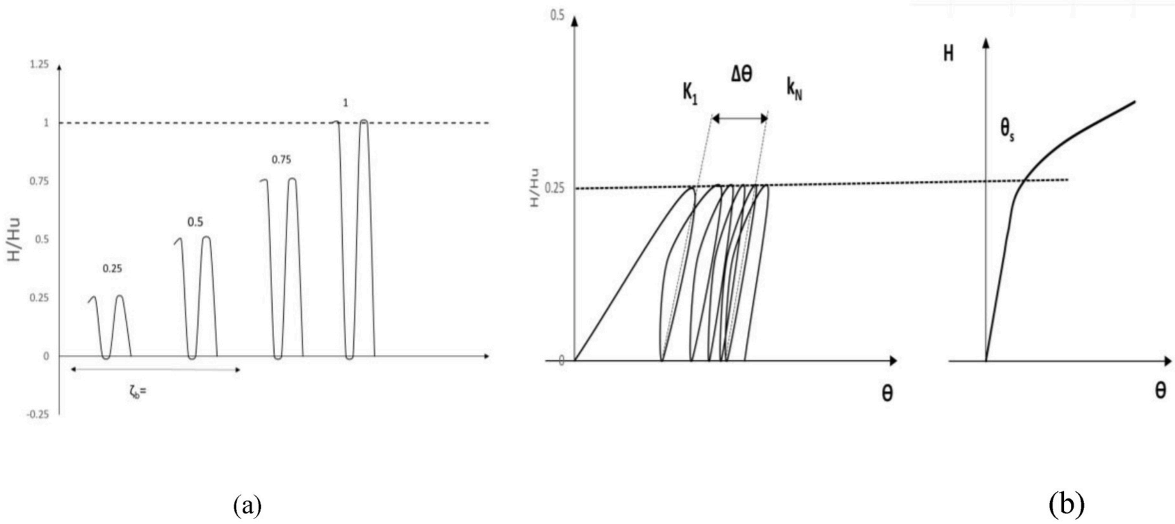

Fig. 2. a) Definitions of ζb and ζc, b) Definitions of k_o, k_N, Θ_o, Θ_N and Θ_S (After LeBlanc et al., 2010).

lateral loading episodes, 3000 cycles each, with varying amplitudes were applied (i.e., 0–30, 0–40, 0–50, and 0–60% of H_u). A similar procedure was followed in the second testing series for the hybrid foundation. It is well known that one-way cyclic loading induces larger displacement and rotation compared to two-way cyclic loading, therefore this was chosen as a worst-case scenario (Hong et al., 2017). Following the notation used by LeBlanc (2010), the used values of the lateral cyclic load ratio ζ_b, which is a ratio of the applied cyclic lateral load (H) to the ultimate lateral load (H_u), were 0.3, 0.4, 0.5 and 0.6. Since the lateral loading was one-way, all tests are done under the condition of $\zeta c = 0$, which is a ratio between the maximum opposite direction lateral load to the mean applied lateral load (Fig. 2a). These tests aimed to establish cyclic degradation envelopes to predict cumulative change in rotation, Θ, and secant stiffness, k, values compared to the first cycle of loading as per Equations (1) and (2), also depicted in Fig. 2b.

$$\Delta\Theta = \frac{\Theta_N - \Theta_1}{\Theta_s} \tag{1}$$

$$\Delta k = \frac{k_N - k_1}{k_s} \tag{2}$$

Since the application of this research concerns offshore wind turbines installed in clays, where the expected soil behavior is undrained due to 1) the nature of the installation, usually driven, and 2) the loading conditions, which typically begin immediately after installation. Hence, to ensure undrained conditions while testing the model foundations, the centrifuge was run at relatively low g levels considering the actuator's available testing speed. This is a direct implication of the centrifuge speed effects on the water seepage velocity and hence the expected response of the foundation due to applied loading. To satisfy the scaling factor between the model and prototype (N), the dynamic time in the model, t_m, should be N times lower than the prototype dynamic time, t_p, i.e. (Admidis and Madbhushi, 2014),

$$t_m = \sqrt{\frac{L_m}{a_m}} = \sqrt{\frac{\frac{Lp}{n}}{a_p * N}} = \frac{t_p}{N} \tag{3}$$

Where L_m and a_m are the model length and acceleration while L_p and a_p are the prototype length and acceleration. Hence, the cyclic loading was performed at a rate of 1.7 Hz at 50g which is equivalent to 0.034 Hz at the prototype scale. Nonetheless, considering the diffusion phenomenon (rate of water volume change with respect to time), compatibility should be ensured between the model and prototype diffusion times. Although high rates can be achieved in the centrifuge, the soil is N times more permeable. Nevertheless, the clay hydraulic conductivity should still be within those of typical fine-grained soils (Madabhushi, 2015).

Table 1
Test matrix.

Test ID	Test ID	Foundation	Description	The eccentricity of load (e), mm	Purpose/ Explanation
Series A	**T1**	Monopile	Monotonic Lateral load	115	Establish lateral capacity, H_u
	T2	Monopile	Monotonic Lateral load	115	Assess the repeatability of T1
	T5	Monopile	Cyclic Lateral loading	115	Assess fatigue limit state- apply 11000 cycles of loading at 30% of H_u
	T6	Monopile	Cyclic Lateral loading	115	Ramp up test- apply 3000 cycles of loading at 30, 40, 50, and 60% of H_u
Series B	**T3**	Hybrid foundation	Monotonic Lateral load	120	Establish lateral capacity, H_u
	T4	Hybrid foundation	Monotonic Lateral load	120	Assess the repeatability of T3
	T7	Hybrid foundation	Cyclic Lateral loading	120	Assess fatigue limit state- apply 18000 cycles of loading at 30% of H_u
	T8	Hybrid foundation	Cyclic Lateral loading	120	Ramp up test- apply 3000 cycles of loading at 30, 40, 50, and 60% of H_u

2.1.1. *Model piles*

The two models were tested in two different boxes (B1 and B2) under laterally applied monotonic and cyclic loading. This paper presents the

Table 2
Model foundation details.

	Properties[a]	Model MP (N = 50g)	Model HF (N = 50g)
Tower	**L_t [m]**	0.14	0.14
	D_t [m]	0.033	0.028
	t_t [m]	0.003	Solid
	Added weight, (g)	87	150
Monopile	**L [m]**	0.143	0.1
	D [m]	0.033	0.022
Plate	**W [m]**	N/A	0.05 0.0145

[a] L: tower length; D_t: diameter of the tower; t_t: the thickness of tower; L_p: pile's length; D: pile's diameter.

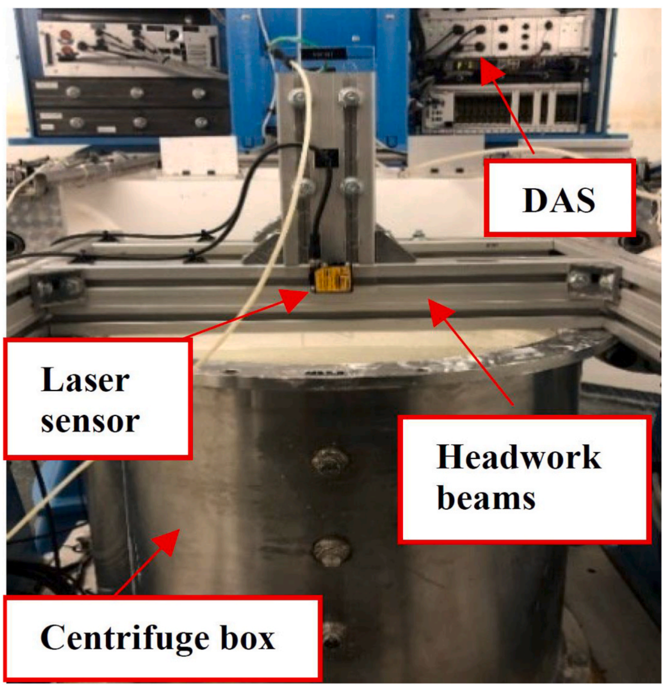

Fig. 3. Centrifuge box and headwork setup.

results of the monotonic and cyclic lateral loading. Table 1 shows the test information. The foundation models were manufactured from acrylic with Young's modulus value of 3.2 GPa. Table 2 presents the model information. In both boxes, the clay bed was consolidated to 70g with a surficial sand surcharge layer of 72 kPa, before the removal of the sand layer and testing at 50g. To establish the stress conditions for cyclic lateral loading episodes in the subsequent tests, each model was pushed to failure under laterally applied loading from a stress-controlled actuator to obtain the lateral ultimate capacity (H_u). The clay profile was probed for shear strength, OCR, moisture content, and unit weight.

2.1.2. Soil sample preparation

The soil used was Speswhite kaolin from Imerys, UK. It has a specific gravity, liquid limit (LL), and plastic limit (PL) of 2.67, 65%, and 30%, respectively. The clay was mixed with water at 1:1.2 by mass in a Winkworth UT150 horizontal shaft vacuum mixer which has a capacity of 150 L for 6 hours to ensure homogeneity. An over-consolidated clay profile was required to provide adequate support for the hybrid foundation plate and to increase the shear strength in the zone of influence of the foundations when laterally loaded. The consolidation process was performed inflight, taking advantage of the increased hydraulic conductivity from the centrifuge scaling laws (Equation (3)).

The centrifuge box has a diameter of 0.5m and a height of 0.53m and is made of steel. To ensure proper drainage, a 4 cm sand layer was placed at the bottom of the centrifuge box and covered with filter paper. Using a plaster scoop, the mixed kaolin slurry was poured into the centrifuge box in thin layers to minimize air entrainment and then left to settle for 24 hours. A 10 cm layer of sand weighing 20 kg was applied over the clay layer to produce the needed over-consolidation ratio (OCR).

The centrifuge box was then loaded onto the beam centrifuge. The consolidation was completed in stages moving from 10g to 70g over a period of 15 minutes to allow for the equalization of pore pressures. Throughout the inflight consolidation phases, the water table was maintained at or slightly above the clay surface to avoid desiccation. The centrifuge was run for three days to prepare the soil bed and ensure approximately 100% primary consolidation. The actual degree of consolidation was obtained based on Taylor's method (Madabhushi, 2015). Subsequently, the centrifuge was spun down and the headwork was removed. Afterward, the sand layer was gently scrapped off and the models were installed at 1g. This is common practice and reported in other studies (Lai et al., 2020; Hong et al., 2017), although it can induce negative skin friction when the clay is reconsolidated before testing. However, this effect may also happen in prototype conditions due to the effects of pile driving (Lai et al., 2020). Fig. 3 shows the centrifuge box and headworks before inflight consolidation. The intended depth of the clay layer after consolidation was 30 cm; therefore, the initial slurry thickness was chosen as 49 cm. Fig. 4 shows a predicted settlement profile used for the purpose of estimating initial and final clay heights.

To increase the efficiency of the tests and maintain quality assurance at the same time, four tests were conducted within one clay sample for each model pile. The first test series involved lateral loading of the MP to establish its ultimate lateral capacity, stiffness properties, and cyclic response. The second series involved conducting similar lateral load tests on the HF (Table 1). These model tests were designed to serve as a baseline for the comparison of the lateral stiffness and capacity of the two foundations. Since wind turbines are subject to vertical (V), lateral (H) and moment (M), VHM loading, it is necessary to apply vertical loading to the model foundations during the lateral load tests. Thus, weights were added to the model tower top representing about 20% of the vertical capacity of the foundation system, which was established using finite element models before the centrifuge tests (Alsharedah, 2022).

2.1.3. Instrumentation

All instrumentation was calibrated to ensure their accuracy and functionality. A load actuator, a load cell, pore pressure transducers, strain gauges, and laser sensors were used to log the test results to the data acquisition system. The pneumatic load actuator used was an SMC type with a load range of up to 7 bars, giving a net load of 375N (Bayton et al., 2018). It was connected with a 200 series in-line load cell calibrated for the expected range of applied load. The structural loads were measured with the load cell and logged into the LABVIEW program with a sampling rate of 5 kHz. The eccentricity of loading (e), with respect to the surface of the soil sample, was 115 mm for both models to produce an equivalent eccentricity for the tests. The laser sensors were Baumer OADM 12U6460/S35A with a reading limit of 104 mm and resolution of 2–120 μm and voltage output between 1 and 10 V. Two laser sensors (Baumer OADM 12) were placed halfway from the box center to record the consolidation data, while two further laser sensors were mounted on a rigid frame system and held opposite to the pile face at 100 mm vertical distance to record lateral displacements and rotations. Both model piles were instrumented with strain gauges (at 2cm/1.5 cm intervals for the MP and HF, respectively) to monitor bending moment evolution with lateral loading. Tokyo Measuring Instruments strain gauges, model GFLA-3-350 were used to measure the bending strains. They were glued to the piles using special adhesive and insulated with a coating to protect against water damage. The strain gauges were oriented in half bridges to double the output and offer temperature compensation. A GoPro

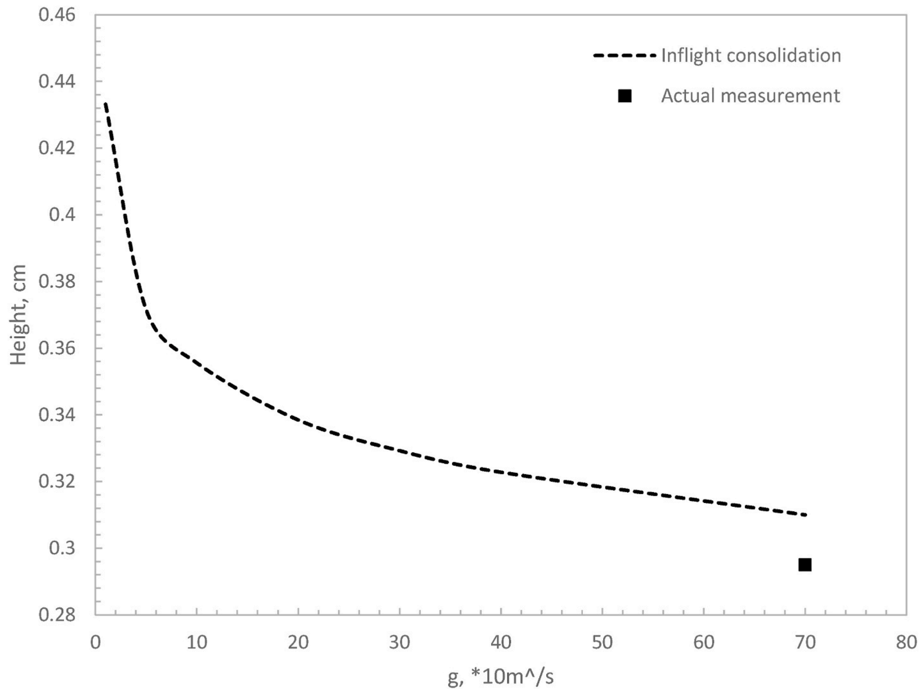

Fig. 4. Settlement versus g level.

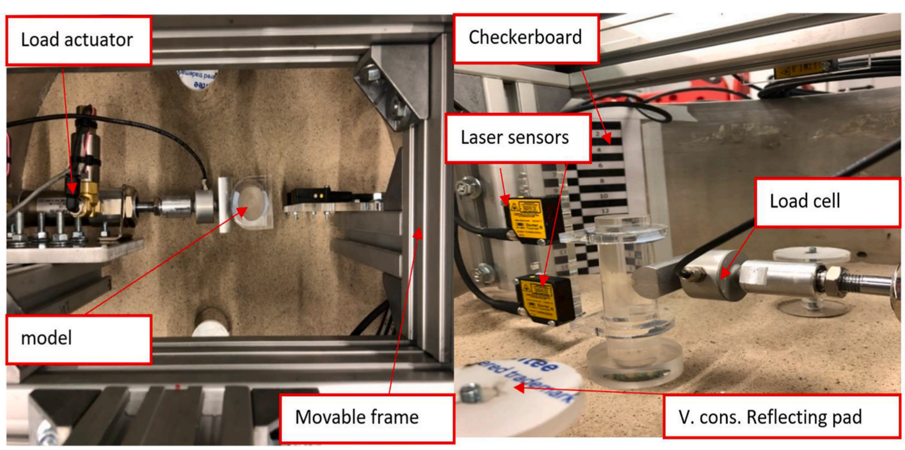

Fig. 5. Top view of headworks and test setup in mock-up test Side view of HF1 showing laser sensors used and load cell and actuator.

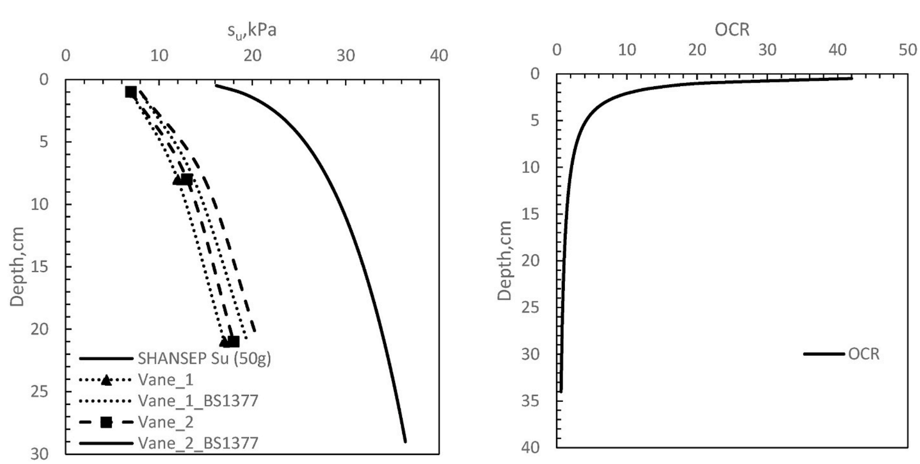

Fig. 6. s_u and OCR profiles.

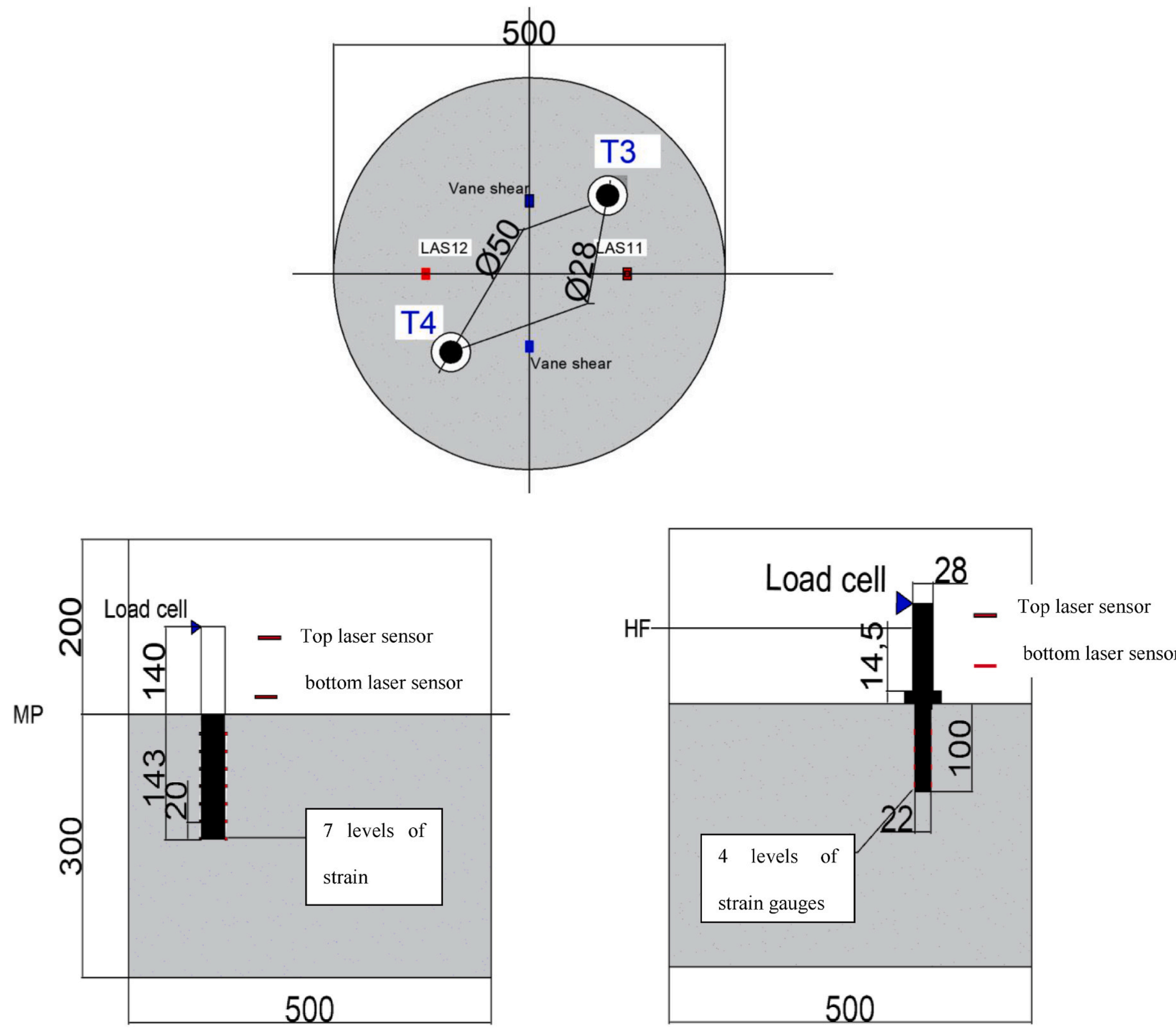

Fig. 7. Tests arrangements, plan and elevation views (dimensions in mm).

Camera was positioned against a laminated checkerboard to monitor the vertical displacement in conjunction with the two vertical laser sensors. The purpose of this is to provide a real-time check of the consolidation progress inflight. Fig. 5 shows the test setup and instrumentation used.

2.1.4. *Vane shear strength and SHANSEP predictions*

To establish the undrained shear strength (s_u) versus depth profile, six vane shear tests were conducted after spin down in the 1g environment at two separate locations (termed BS-1377 in Fig. 6 with BS referring to British Standard). The vane shear tests were carried out with a vane apparatus having a diameter of 19 mm. The adopted shearing rate ensured that failure is reached within 10 seconds (ASTM D8121/ D8121M). The tests were conducted at 7, 12, and 21 cm depth below the clay surface at the two locations shown in Fig. 7 and were normalized against OCR to establish the shear strength parameters. The OCR was estimated from the soil unit weight and pre-consolidation pressure from the sand surcharge, while moisture content measurements were retrieved from pressed-in tube samples. To map the shear strength data to get the s_u versus depth profile at the g level used for testing, the s_u at 1g was the best fit according to the SHANSEP procedure, Equation (4).

$$s_u\ (\mathrm{SHANSEP}) = C_1 \ * \sigma' \ * OCR^{C_3} \tag{4}$$

where: C_1 and C_3 are fitting parameters and range between (0.18–0.35) and (0.51–0.9).

Having accomplished this, the s_u profile can be established for any g level knowing the soil's effective stress and OCR values. From the best-fit equation, the C_1 and C_3 parameter values were found to be 0.325 and 0.8, respectively. Hence, the shear strength profile at 50g was estimated. Fig. 6 shows the predicted shear strength profile at 50g employing Equation (4) and using fitting parameters C_1 and C_3. As shown in Fig. 6, a parabolic soil shear strength profile was established with the consolidation process, which indicated consistent shear strength data with the measured values at 1g and agrees well with previous researchers' predictions of over-consolidated Kaolin clays, such as those presented by Alnuaim (2014). A parabolic variation of s_u was accomplished which is typical for over-consolidated clays (Hong et al., 2017; Lau, 2015; Zhang et al., 2011).

2.1.5. *Consolidation and shear strength profile*

Inflight consolidation indicated soft soil with an average compression index of 0.49 and a rebound index of 0.07. Fig. 6 shows the s_u and OCR profiles after consolidation. The coefficient of consolidation, $c_{v,}$ of the clay, was estimated to be 8E-7 m^2/s, while s_u and OCR varied from 15 to 40 to 36-1 between the surface and the base of the box, respectively.

It can be seen from Fig. 6 that the shear strength profile obtained is realistic with shear strength increasing at a rate of 3 kPa/m at shallow depths due to the effects of over-consolidation ratio and eventually decaying to about 0.5 kPa/m with the surficial shear strength (s_{uo}) and OCR values being around 15 kPa and 42, respectively. The average shear strength in the mobilized zone, which consists of the soil mass

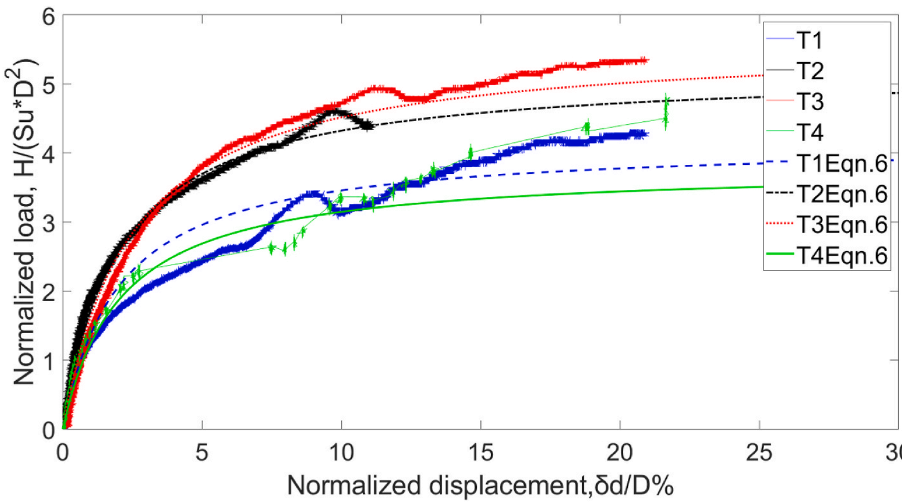

Fig. 8. Load versus displacement plots at top laser sensor.

responsible for resisting the majority of the applied loads (typically being 6 diameters for monopiles under lateral loading conditions) is around 22 kPa.

2.2. Test package arrangement

Test arrangements were carefully planned to maximize the benefits of the centrifuge setup and allow efficient and quick changes between tests. Two test boxes were prepared, one for each model following the same procedure to produce similar soil profiles.

A point load was applied to the model towers (free to rotate) using the pneumatic actuator which was rigidly attached to the headwork beams to ensure perpendicular alignment with, and full load application on the model foundations. The rate of lateral loading was estimated based on Equation (5) to produce an undrained response (Hong et al., 2017).

$$V\ (\mathrm{mm/sec}) = \frac{20 * c_h}{B} \tag{5}$$

where c_h is the soil lateral coefficient of consolidation while B is the characteristic length of the structure. The c_h values can vary significantly with respect to c_v, with c_h being an order or several in magnitude higher than the c_v in some soil conditions, depending on the geological and deposition history. Due to the quick consolidation process in the centrifuge and the available 2-way drainage conditions, c_h is taken equal to c_v. For the MP, B was taken as D, while for the HF B was taken as the average diameter of the plate width and the pile diameter. The test locations of the models were placed more than 7D apart within the box and were situated at least three times the monopile diameter (D) or HF plate width (W) from the box rigid boundary, which was deemed to be sufficient to avoid boundary influences (Zhang et al., 2017; Hong et al., 2017). Fig. 7 shows a plan view of the box and locations of the tests T3 and T4 in box 2. A similar testing procedure is followed in T1 and T2 for the MP in box 1. Tests 5/6 and Tests 7/8 were conducted in the opposite locations of T1/2 and T3/4, respectively.

3. Results

3.1. Monotonic loading

Fig. 8 shows the load-displacement curves from the monotonic tests. The foundations' lateral ultimate capacities were taken as the highest reached values from Equation (6). In all tests, the load-deflection curve showed a hyperbolic shape, i.e., increasing initially linearly at small deflection and showing progressive yielding as displacement increased. This is typical behavior for most foundations and is a result of the soil elastoplastic response (Chen and Xu, 2016). The results can be fitted using a hyperbolic curve of the form (Kulhawy and Chen, 1995):

$$\mathrm{H} = \frac{d}{a + bd} \tag{6}$$

where H is the applied lateral load, d is the measured deflection, and a and b are the reciprocal of the initial stiffness and ultimate capacity, respectively.

At small displacements, the soil experienced correspondingly small strains and the response was in the elastic region. As the load increased, the strain level in the soil around the foundations increased giving rise to plastic deformations and decreased stiffness response, eventually leading to plastic flow at ultimate loads. The average normalized lateral ultimate capacity values, $H_u/(s_u{*}D^2)$, were 4.0 for the monopile and 4.5 for the hybrid foundation occurring at a normalized deflection, δd/D%, of 10.6% and 20.5%, respectively (Fig. 8). This variation in capacity and shear strain may be attributed to the loading rate difference between tests, installation disturbance, and consolidation effects. For instance, Test T2 was performed after conducting T1, which may have resulted in a stiffer soil profile due to reconsolidation occurring between each test. Test 4, however, was conducted after T3 and showed "smaller capacity". This may be a result of installation effects and contact conditions between the plate and mudline. The average initial stiffness values were 77.6 N/mm (3.8 MN/m) and 47 N/mm (2.35 MN/m) for the MP and HF, respectively. Although the MP showed a stiffer response, the HF system, with a smaller diameter and lesser embedment, continued to offer resistance at higher mobilized lateral straining. This improvement in lateral response with the hybrid foundation is believed to originate from the soil-structure interaction. It is believed that the soil structure interaction (SSI) of the plate-soil-pile resulted in an increased stiffness and lateral capacity response of the HF system providing comparable behavior with the MP counterpart. It is well known that the soil shear strength is stress dependent. With lateral load being applied with eccentricity (relative to the plate), part of the plate experiences increased stresses leading to increased shear resistance not only at the plate level but also on the pile front. The increase in stiffness, although not high as the increase in H_u, can also be indicative of the HF performance at serviceability loads. Fig. 8 also displays the normalized load-deflection curves obtained from Equation (6).

3.2. Cyclic loading

Since one of the objectives of this research is to evaluate the response

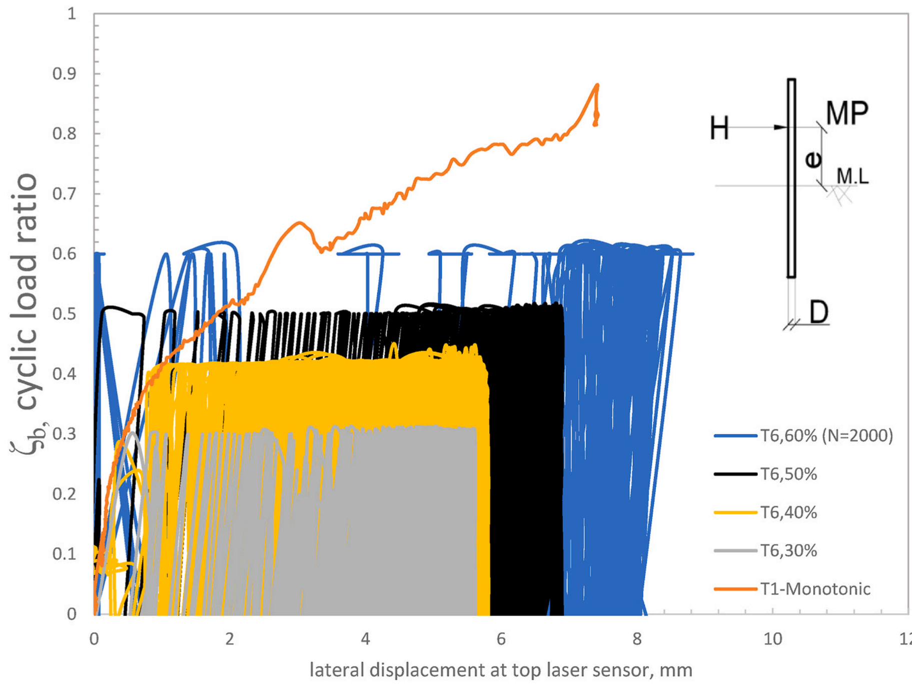

(a)

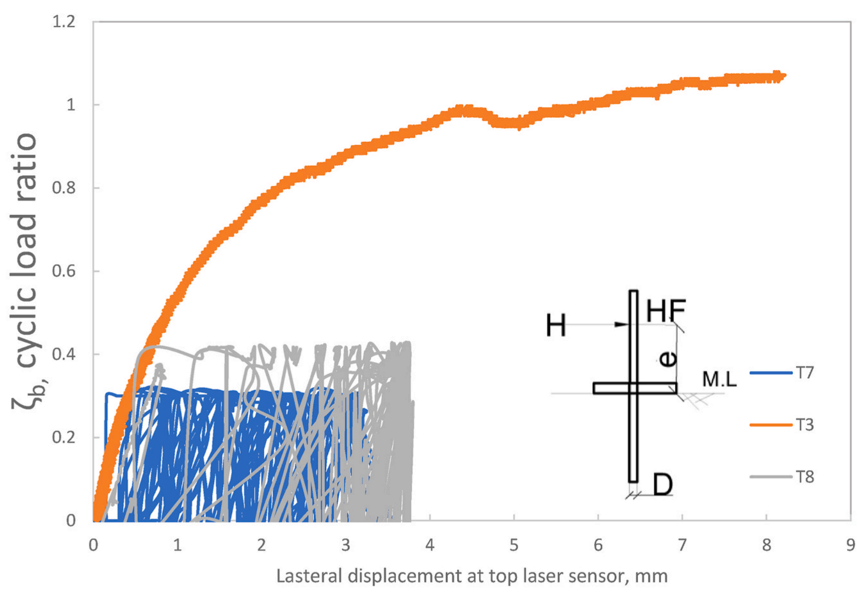

(b)

Fig. 9. Cyclic load displacement curves (measured with top laser sensor) for (a) Monopile (b) Hybrid foundation. (up to 3000 cycles).

of the MP and HF under laterally applied cyclic loading, a series of tests were considered to obtain a glimpse of the two foundation's response characteristics under these loading conditions. Herein we shed light on the results of such tests and discuss the results of Tests 5/6 and Tests 7/8. The goals of these tests were two-fold, namely: 1) to establish the effects of the loading regime ($\zeta_b = 0.3$ to $\zeta_b = 0.6$, $\zeta_c = 0$) on the stiffness values and the rotation of the considered systems, and 2) to best fit the centrifuge test results with predictive equations for practical applications. The lateral stiffness and rotation were normalized against the values of the first cycles according to Equations (1) and (2). Fig. 9 presents the cyclic load-displacement curves of the MP and HF. It can be seen from Fig. 9 that the cyclic loading-displacement curves indicate progressive accumulation of displacement, and hence rotation, with cyclic loading for all loading regimes ($\zeta_b = 0.3$ to $\zeta_b = 0.6$). However, the magnitude of accumulation is dependent on the magnitude of the cyclic loading ratio as lower accumulation rates were found with lower values of ζ_b.

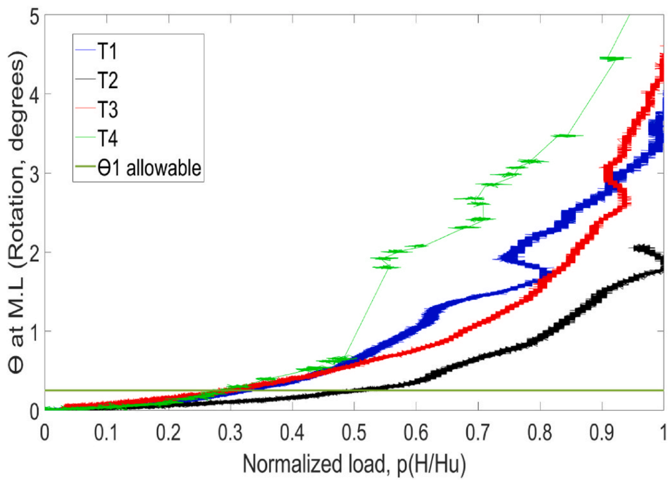

Fig. 10. Rotation evolution at M.L versus normalized load, p.

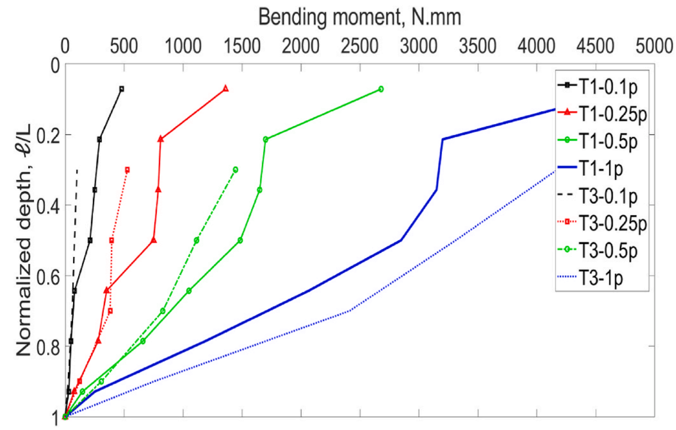

Fig. 11. Bending moment profiles versus normalized depth for the MP(T1) and HF(T3).

3.3. Discussion of monotonic loading tests

The monopile was loaded at a 115 mm eccentricity above the mudline with the load-controlled actuator. The strain rate of loading for the MP inferred from the load-displacement curve and the load time graph indicated that the normalized loading rate, $\beta = (V^*D)/c_h$, the value was between 2.4 and 5.7, where c_h is the horizontal coefficient of consolidation (taken as equal to c_v), D is the diameter and V is the loading rate (Finnie and Randolph, 1994). These values fall within the range of undrained loading. As the lateral loading proceeds, the pile face moves towards the soil and generates pressure on the soil both from pure shearing at the pile edges and a combination of shear and compressive loading. This pressure is transferred to the soil pushing it outwards, forming a gap with increased loading behind the pile. Under this high rate of loading, excess pore pressure is generated giving rise to undrained behavior. This is believed to be a worst-case scenario, as offshore wind turbines are typically exposed to lower-speed wind loads for most of their lifetime, with fewer major storm loads (Yu et al., 2019). These wave and wind loads often fall between the fully drained and undrained loading cases, therefore potentially increasing the soil strength and stiffness with time.

The MP behavior can be classified as either flexible, rigid, or semi-depending on the relative rigidity of the MP compared to the soil. Poulos and Hull (1989) defined upper and lower bound values of $E_pI_p/(E_sL^4)$ for flexible and rigid piles as being 0.0025 and 0.208, respectively where E_p, I_P, E_s, and L are Young's modulus, second moment of inertia, soil stiffness and pile's length, respectively (Hong et al., 2017). Assuming the E_s value is 400 s_u, the pile has an $E_pI_p/(E_sL^4)$ value of 0.109, which is between these limits classifying the pile as semi-rigid. Fig. 11 shows the bending moment diagrams versus normalized depth ℓ/L under different load levels from Test T1 (blue line in Fig. 8). It can be observed that the pile rotation and tilting are uniform across the height and the bending moment shows no sign of rotation and zero toe bending, which is the typical behavior for rigid piles (Zhang et al., 2011; Wang et al., 2018; Byrne et al., 2015; Lau, 2015; Lai et al., 2020).

The hybrid foundation was loaded at 120 mm eccentricity above the mudline. The strain rate of loading for the HF inferred from the load-displacement curve and the load time graph indicated that the normalized loading rate, $\beta = (V^*D)/c_h$, value is between 6.8 and 8.7. Again, these values fall within the range of undrained loading. As the lateral loading proceeds, the plate rotates around its axis generating restoring moments from the soil pressure and increasing pressure in front of the pile face, all contributing to the resistance against the applied lateral loads. Under such a high rate of loading, excess pore pressure is generated giving rise to undrained behavior. Repeated applied loading may cause differential settlement underneath the plate. To avoid these conditions, it is important to have the plate penetrate through the mudline to prevent separation from taking place, although this is beyond the scope of this study. Fig. 11 shows the bending moment diagram for the HF versus normalized depth ℓ/L (Test T3, red line in Fig. 8) under different loads. It can be observed that the pile is exhibiting a similar bending moment profile to that of the rigid pile as the bending moment diagram shows no sign of flexure occurring and zero toe bending, which is also the typical behavior of rigid piles (Zhang et al. (2011); Wang et al. (2018); Lau (2015); Lai et al. (2020)). Fig. 11 shows that for higher loading conditions, the HF showed smaller or similar bending moments to the MP, which can be viewed as a benefit of the system potentially reducing the pile size and minimizing steel use; this resulted from the interaction of the plate mitigating some of the shear loads transferred to the hybrid foundation's pile.

A key point for OWTs is serviceability and therefore we have compared the evolution of rotation with applied loading. Since the capacities of the systems are close to one another, they were normalized from 0 to 1 ($p = H/H_u$) where H represents lateral applied load and H_u denotes the highest recorded lateral load. Fig. 10 shows that as the load progressed, the MP and HF rotations increase at similar rates. However, at a serviceability loading value of 0.2, the MP and the HF show similar trends. Therefore, from this point of view, the HF has the potential and effectiveness to replace specific MPs with smaller piles and associated bending moments. Also, Fig. 10 shows the allowable rotation for the first cycle of loads, Θ1, which is usually taken as 0.25^0 (Malhorta, 2009).

3.4. Discussion of cyclic loading tests

Fig. 9a shows the results of Tests 5/6 and Fig. 9b shows the results of Tests 7/8. The monotonic curves are superimposed on the results. From Fig. 9a and b, it can be seen that the cyclic results closely follow the monotonic curves in the first cycle for the initial episode of loading ($\zeta_b = 0.3$). It can also be observed that the effects of the preceding cycles on the stiffness properties are significant. From Fig. 9a, it is evident that the cyclic loading on the monopile led to increased displacement and hence rotation with cycling. As the test setup included two laser sensors at different heights, the angular rotation at the mudline can be measured from the laser sensors directly. The rotation and stiffness values Θ_1 and k_1 were obtained from the first cycle as shown in Fig. 2. After that, the θ_N value is obtained and normalized against angular rotation from the monotonic tests, θ_s, and plotted against the logarithm of the number of cycles, Equation (1). By doing so, one can observe that the results can be fitted to a linear function of the form:

$$\frac{\Delta\theta}{\theta_s} = T_c\ (\zeta_c) * T_b\ (\zeta_b)\ * N^{\alpha} \quad (7)$$

T_b and T_c are dimensionless values and are based on the load

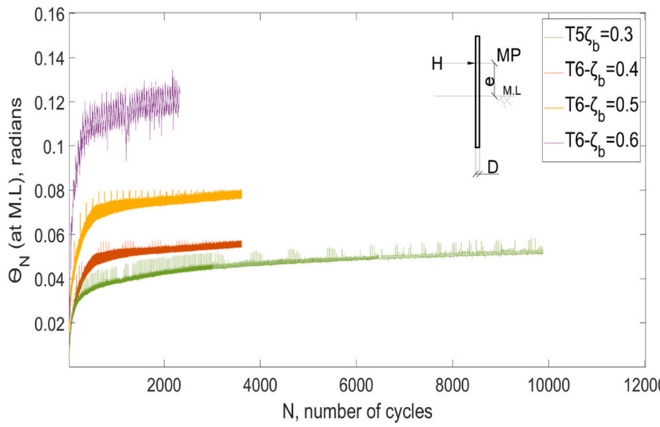

Fig. 12. Rotation evolution at M.L vs. number of cycles.

characteristics, see Fig. 2 (after Leblanc, 2010). As the load considered in this paper is one-way, T_c (ζ_c) is taken as unity. By fitting the results of T5, T6, T7, and T8, the values of T_b (ζ_b) and α are determined. For the HF, Equation (7) did not yield a good fit and hence another form of equation was used. The equation in this case has the following form;

$$\frac{\Delta\theta}{\theta_s} = b + \log(N)^{\alpha} \tag{8}$$

where b and α are constants. Fig. 12 displays the rotation evolution with the number of cycles for the MP from Tests 5 and 6. In Test 5, the MP underwent 9000 cycles of loading under fatigue conditions. In Test 6, the cycling amplitude, ζ_b, was varied as 0–30%, 0–40%, 0–50%, and 0–60% for around 3000 cycles. In the first episode, the strain adjacent to the pile was small, and a shakedown response was obtained after 1060 cycles, with the results confirming the trends observed in Test 5. In the second episode, the same pattern was noticed as in episode 1, although with greater changes in rotation rate versus cycle number. It is also observed that the first cycle's initial stiffness has increased significantly due to possible reconsolidation between the consecutive episodes of cycling. This is also to be expected in field conditions as OWTs are subjected to cyclic loads throughout their lifetime and reconsolidation is anticipated to take place (although at varying degrees depending on drainage conditions). A shakedown response was also noted for ζ_b = 0–50%, however at a different rate of rotation change and cycle number. During cyclic loading with ζ_b = 0–60%, the pile experienced a ratcheting response, i.e., the rotation increased almost linearly with the number of cycles. Gaps formed in front of the pile in the last episode. Plotting the data on a log-log scale shows the normalized rotation follows an almost linear function of log(N). This suggests a power law relationship

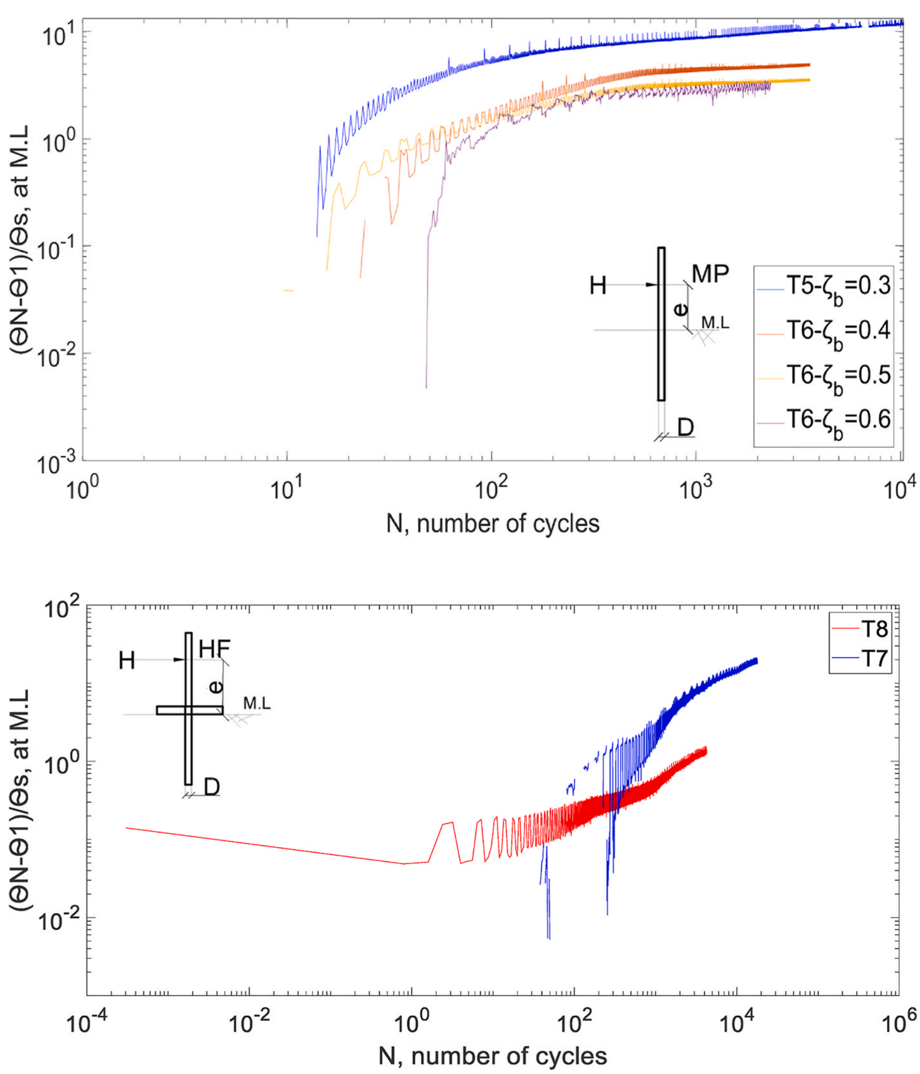

Fig. 13. Normalized rotation at mudline versus logN for MP and HF.

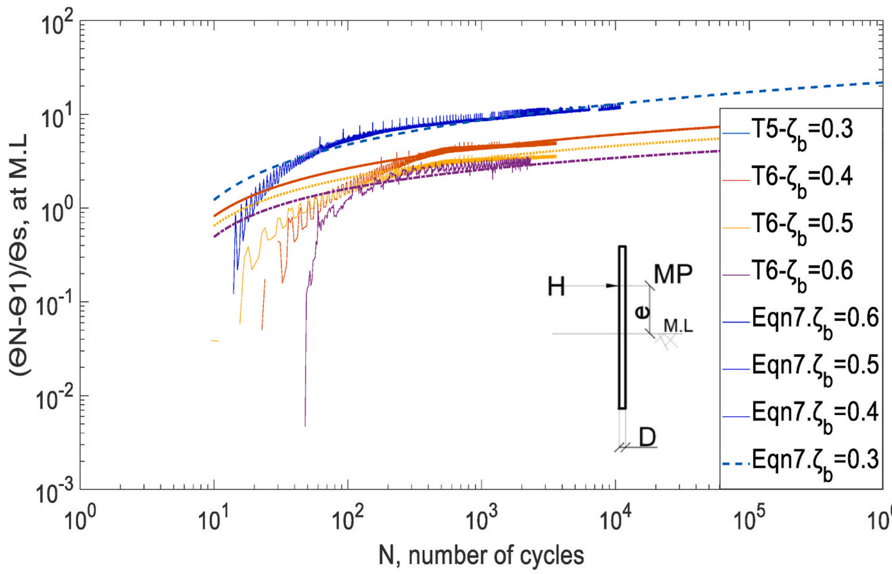

a)

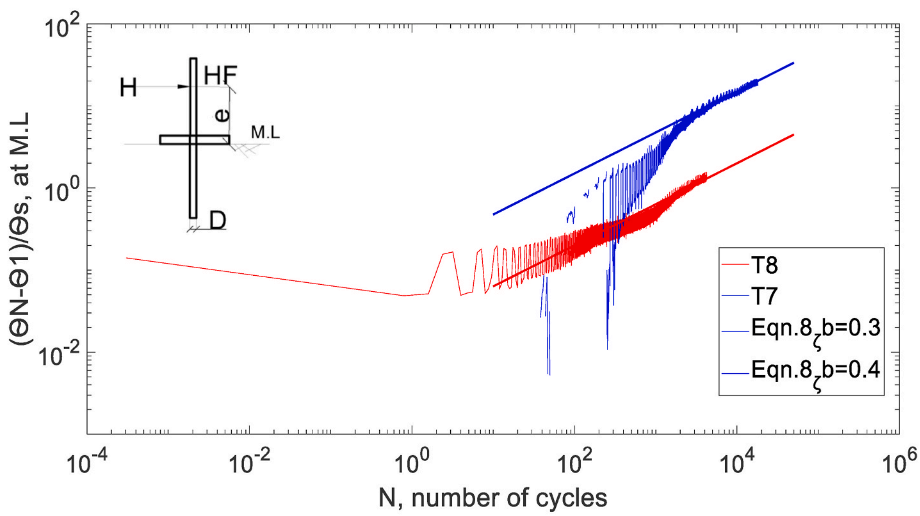

b)

Fig. 14. Effects of cyclic regime and number of cycles on the rotation evolution at mudline with predictive equations for a)MP, b) HF.

Table 3
Fitting Equations for cyclic degradation for MP.

Foundation Type	Load regime	B	α	N Limitation
MP	0.3	−1.5	1.2	100–100000
	0.4	−1.3	0.9	100–100000
	0.5	−1.3	0.8	100–100000
	0.6	−1.3	0.7	100–100000

Table 4
Fitting Equations for cyclic degradation for HF.

Foundation Type	Load regime	T_b	α	N Limitation
HF	0.3	0.15	0.5	10–100000
	0.4	0.02	0.5	10–100000

between θ and N. Similar observations are reported by Byrne et al. (2013) who found that the accumulated rotation due to cyclic loading can be expressed as a function of T_b and N^{α}, where the value of αwas 0.39 (LeBlanc et al., 2010). Fig. 13 presents the normalized rotation of the MP at the mudline versus the number of cyclic lateral loading episodes following the notations in Equation (2).

Fig. 14 displays the rotation accumulation at mudline versus number of cycles from the test results and from Equation (7)/8 and Tables 3 and 4 for both MP and HF foundation systems. Tables 3 and 4 present the fitting parameters used to construct Fig. 14.

3.5. Unloading stiffness

Being cyclically loaded, it is important to monitor the evolution of the lateral stiffness of the offshore wind turbine. It is well known that the first natural frequency of OWTs affects their fatigue life because of resonance concerns. Hence, this section discusses the changes in the lateral stiffness properties of the considered systems due to the imposed

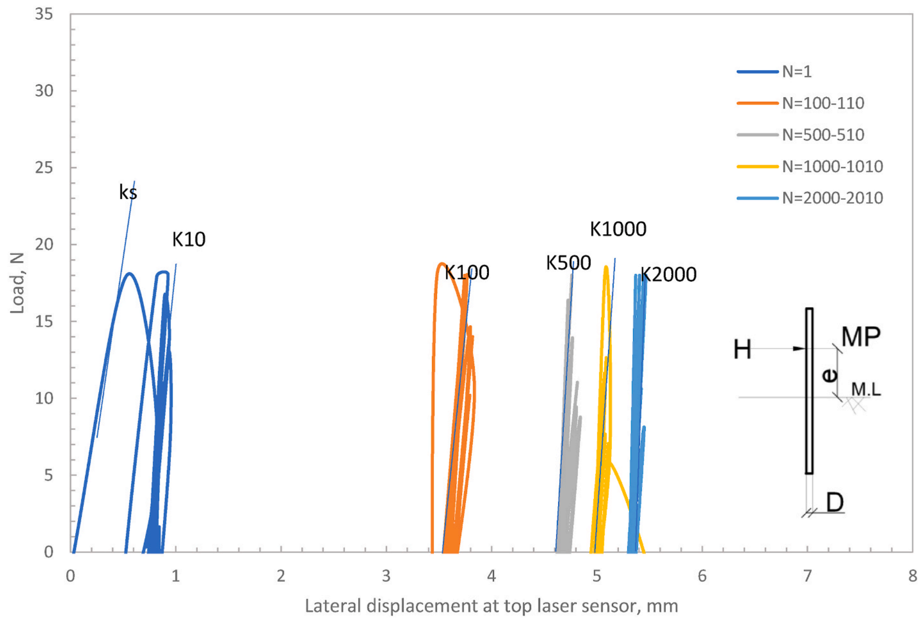

Fig. 15. Selected episodes (N) showing progressive softening response of monopile under cyclic loading ζb = 0.3 (T5).

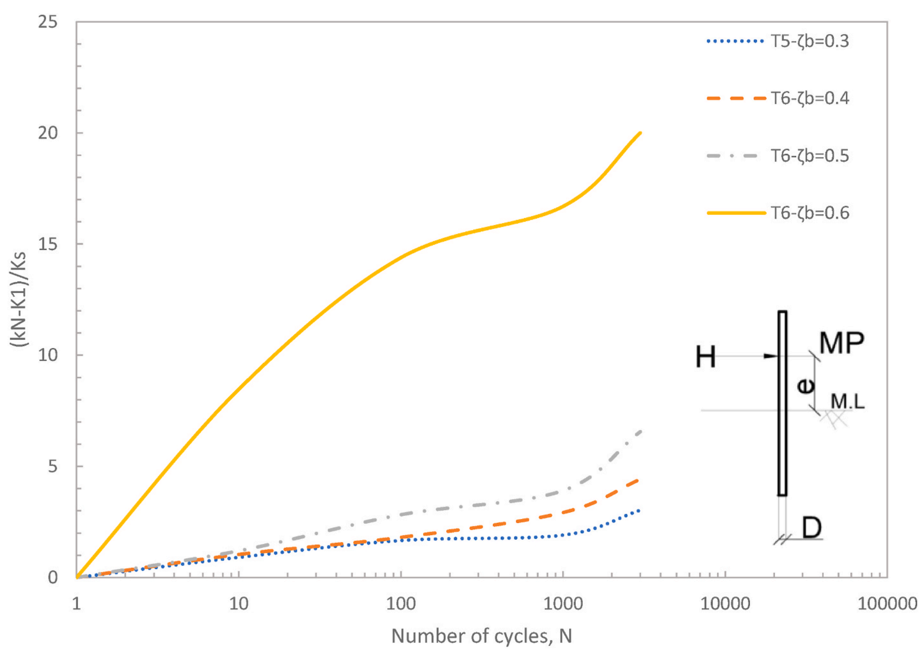

Fig. 16. The rate of change of secant stiffness of MP under various loading characteristics (T5 and T6).

loading regime. As shown in Fig. 9a and b, there is an elastic and plastic (permanent) component to the lateral deflection at certain cyclic loading levels. This occurred due to the progressive softening of the clay resisting the cyclic loading and the resulting excess pore pressure. This pore pressure change can be positive or negative depending on the stress history of the soil, mean effective stress, stress increase, and soil fabric. The shear modulus of the soil is dependent on the mean effective stress, OCR, and soil type, hence a reduction in the mean effective stress causes reductions of the shear modulus value, G, leading to progressive displacement and rotation with cycling. Also, increased cycling can lead to gap opening which appeared to occur in the tests resulting in decreased stiffness properties. Furthermore, long-term cycling can induce changes in the clay structure and alter the void ratio, which results in changes to the shear modulus of the clay. The cyclic loading conducted considered the dynamic scaling of the applied load; nevertheless, the pore fluid was water which may have caused partial consolidation during cycling and may explain the increased stiffness response (decaying rate of change of plastic strains with cycles, termed shakedown). Nonetheless, a higher applied stress ratio of $\zeta_b = 0$–60% resulted in a ratcheting response, which can be attributed to the strain response of the clay being stress-dependent. Fig. 15 shows the effects of cycling on the monopile response under 30%H_u. It can be observed that the cyclic loading led to an increased stiffness response (secant stiffness). The response of OWTs to cyclic loading is expected to be frequency dependent, and codes of practice such as DNV recommend that the loading frequency must be ±10% away from forcing frequencies (DNV, 2014). Given the frequency is the square root of the stiffness divided by the mass, an increase of 200% in the lateral stiffness value of the structure, k_L, will result in a frequency change of more than 40%. This is a problematic situation that can lead to various structural issues and damage to the turbine components. Fig. 16 shows the normalized stiffness change versus number of cycles. It is evident that the applied cyclic loading caused an increased stiffness response in all cyclic episodes, with the highest rate of change resulting from the highest loading magnitude. Given the likelihood of more severe cycles occurring in the lifetime of OWTs is small, the expected stiffness change lies between 100 and 400%. This translates to a 10–40% increase in the first natural frequency for the soft soil considered herein. This change can result in frequency interference between the OWT and the forcing frequencies of 1P, rotor frequency, and 3P, blade passing frequency.

4. Conclusions

Models representing the MP and HF systems have been scaled from prototypes to study their behaviour under monotonic and cyclic lateral loading. The two models were pushed monotonically to failure laterally and their lateral ultimate capacity and response under equivalent working conditions were examined. The models were tested at 50g in an over-consolidated kaolin clay under undrained loading conditions, and the following conclusions have been drawn:

1) The hybrid foundation (HF) with L_p/W of 2 offered a similar capacity to a monopile (MP) at reduced L_p and pile diameter.
2) The observed bending moments indicated rigid behavior for all models with no flexing. due to the high used $E_pI_p/(E_s L^4)$ values.
3) At higher lateral loads, the HF pile experienced similar bending moments as the MP due to the interaction of the plate with the soil and the pile. This indicates that the HF can prove advantageous in resisting lateral loads with improved distribution of stresses rendering efficient use of structural materials.
4) The soil structure interaction (SSI) improved the hybrid foundation response to lateral loading through the distribution of loading into shear loads underneath the plate, passive soil pressure in front of the pile, and through imparted resisting moment from the plate
5) At the same load, the MP offered increased stiffness response and less rotation at the mudline compared to the HF. This is due to the weak soil conditions underneath the plate. A stiffer HF response is expected with stiff clay sites and near surface consolidation beneath the plate following construction. This can be beneficial when pile driving is an issue and smaller piles are more practical.
6) A series of cyclic episodes were applied to the MP and HF. Under cyclic lateral loading, the MP continued to record increase rotations, however, at decaying rates.
7) For a given number of cycles, the rotation magnitude increased with increase of cyclic loading ratio ζ_b.
8) By normalizing the cyclic rotation by the static rotation at the same loading magnitude and plotting against log N, a linear relationship was found. Fitting the rotation vs. log(N) by Equation (7) or 8, a number of damage accumulation relationships are proposed.
9) For the texted ranges of ζ of 0–30 and 0–40%, the MP experienced shakedown response. The N value beyond which a minimal increase in rotation was noticed to increase as the ζ value rises and was 1060 and 1300 for ζ values of 0–30% and 0–40%, respectively.
10) Under cyclic lateral loading, the HF continued to record increase rotations, however, at decaying rates. The rotation magnitude increased with an increase of the cyclic loading ratio ζ.
11) For the tested ranges of ζ of 0–30% and 0–40%, the HF experienced a shakedown response. The N value beyond which a minimal increase in rotation was noticed to increase as the ζ value increased and was 1200 and 1470 for ζ values of 0–30% and 0–40%, respectively.

CRediT authorship contribution statement

Yazeed A. Alsharedah: Conceptualization, Interpretation, Writing – original draft, preparation. **Jonathan A. Black:** Methodology, Software, Data curation, and, Tests execution. **Timothy Newson:** Supervision, Writing – review & editing. **M.H. El Naggar:** Supervision.

Declaration of competing interest

The authors declare that they have no known competing financial interests or personal relationships that could have appeared to influence the work reported in this paper.

Data availability

The authors do not have permission to share data.

Acknowledgments

The researchers would like to thank the Deanship of Scientific Research, Qassim University for funding the publication of this project.

Appendix A. Supplementary data

Supplementary data to this article can be found online at https://doi.org/10.1016/j.oceaneng.2023.115421.

References

Abdelkader, Ahmed Mohamed Reda, 2016. Investigation of Hybrid Foundation System for Offshore Wind Turbine (Scholarship@Western).
Alnuaim, A.M., 2014. Performance of Micropiled Raft in Sand and Clay-Centrifuge and Numerical Studies. School of Graduate and Postdoctoral Studies, University of Western Ontario, 2014.
Alsharedah, Y., 2022. Behaviour of Monopile and Hybrid Foundations for Offshore Wind Turbines: Centrifuge Testing and Numerical Modelling. Thesis and Dissertation Repository UWO.
Bayton, S., Black, J., Klinkvort, R., 2018. Centrifuge modelling of long term cyclic lateral loading on monopiles. In: Physical Modelling in Geotechnics, first ed. Routledge, pp. 689–694. https://doi.org/10.1201/9780429438660-103.
Black, J., Baker, N., Ainsworth, A., 2014. Establishing a 50 g-ton geotechnical centrifuge at the university of Sheffield. In: Proceedings of the 8th International Conference on Physical Modelling in Geotechnics (Perth, Aus).
Byrne, 2013. Foundations for Offshore Wind Turbines. Presentation. University of Oxford.
Byrne, B.W., Houlsby, G.T., 2003. Foundations for Offshore Wind Turbines", vol. 361. Philosophical Transactions of the Royal Society of London, Series A, December, pp. 2909–2930.
Byrne, B.W., McAdam, R., Burd, H.J., Houlsby, G.T., Martin, C.M., Zdravković, L., Taborda, D.M.G., Potts, D.M., Jardine, R.J., Sideri, M., Schroeder, F.C., Gavin, K., Doherty, P., Igoe, D., Muir Wood, A., Kellahave, D., Skov Gretlund, J., 2015a. New design methods for large diameter piles under lateral loading for offshore wind applications. Proceedings of Third International Symposium on Frontiers in Offshore Geotechics 1, 705–710.
Byrne, B.W., McAdam, R., Burd, H.J., Houlsby, G.T., Martin, C.M., Gavin, K., Doherty, P., Igoe, D., Zdravković, L., Taborda, D.M.G., Potts, D.M., Jardine, R.J., Sideri, M., Schroeder, F.C., Muir Wood, A., Kellahave, D., Skov Gretlund, J., 2015b. Field testing of large diameter piles under lateral loading for offshore wind applications. In: Proceedings of XVI European Conference *on* Soil Mechanics and Geotechnical Engineering, pp. 1255–1260. Edinburgh.
Chen, Xu, Z., 2016. Deflection measurement of bored pile body with steel bar meters in the lateral load test. Geotechnical Testing Journal 39 (2), 315–323. https://doi.org/10.1520/GTJ20150136.
Cherchia, M., 2016. Centrifuge Modeling of Hybrid Foundations for Offshore Wind Turbines.
DNV, 2014. Offshore Standard DNV-OS-J101 Design of Offshore Wind Turbine Structures. Høvik, Norway.
El-Marassi, M., El Naggar, M.H., Newson, T., Stone, K., 2008. Numerical Modelling of the Performance of a Hybrid Monopiled-Footing Foundation. GeoEdmonton.
Finnie, I.M.S., Randolph, M.F., 1994. Punch-through and liquefaction induced failure of shallow foundations on calcareous sediments. In: Proceedings of the International Conference on Behavior of Offshore Structures. BOSS), Boston, Mass, pp. 217–230.
Hong, Y., He, B., Wang, L.Z., Wang, Z., Ng, C.W.W., Mašín, D., 2017. Cyclic lateral response and failure mechanisms of semi-rigid pile in soft clay: centrifuge tests and numerical modelling. Can. Geotech. J.
Kulhawy, F.H., Chen, 1995. A Thirty-Year Perspective of Broms' Lateral Loading Models, as Applied to Drilled Shafts. In: The Bengt B. Broms Symposium on Geotechnical

Engineering, December 13–15, 1995. NTU-PWD Geotechnical Research Centre, Singapore, pp. 225–240.
Lai, Y., Wang, L., Hong, Y., He, B., 2020. Centrifuge modeling of the cyclic lateral behavior of large-diameter monopiles in soft clay: effects of episodic cycling and reconsolidation. Ocean Eng. 200, 107048 https://doi.org/10.1016/j.oceaneng.2020.107048.
Lau, B., 2015. Cyclic Behaviour of Monopile Foundations for Offshore Wind Turbines in Clay. ProQuest Dissertations Publishing.
Lehane, B.M., Pedram, B., Doherty, J.A., Powrie, W., 2014. Improved performance of monopiles when combined with footings for tower foundations in sand. J. Geotech. Geoenviron. Eng. 140 (7), 4014027 https://doi.org/10.1061/(ASCE)GT.1943-5606.0001109.
Lombardi, D., Bhattacharya, S., Muir Wood, D., 2013. Dynamic soil–structure interaction of monopile supported wind turbines in cohesive soil. Soil Dynam. Earthq. Eng. 49, 165–180. https://doi.org/10.1016/j.soildyn.2013.01.015, 1984.
Madabhushi, G., 2015. Centrifuge Modelling for Civil Engineers, first ed. CRC Press. https://doi.org/10.1201/9781315272863.
Malhotra, S. "Design and Construction of Offshore Wind Turbine Foundations," Wind Turbines, pp. 231-264.
Powrie, W., Daly, M.P., 2007. Centrifuge modeling of embedded retaining walls with stabilizing bases. Geotechnique 57 (6), 485–497.
Stone, K., Newson, T., Sandon, J., 2007. An investigation of the performance of a 'hybrid' monopile-footing foundation for offshore structures. In: Proc. 6th Int. Conf. Of the Society of Underwater Technology, pp. 391–396. London.
Wang, X., Zeng, X., Yang, X., Li, J., 2018. Feasibility study of offshore wind turbines with hybrid monopile foundation based on centrifuge modeling. Appl. Energy 209, 127–139. https://doi.org/10.1016/j.apenergy.2017.10.107.

Update

Ocean Engineering

Volume 291, Issue , 1 January 2024, Page

DOI: https://doi.org/10.1016/j.oceaneng.2023.116583

Ocean Engineering 291 (2024) 116583

Contents lists available at ScienceDirect

Ocean Engineering

journal homepage: www.elsevier.com/locate/oceaneng

Corrigendum to "Centrifuge testing of improved monopile foundation for offshore wind turbines" [Ocean Eng. V285 part 2 (2023) 115421]

Yazeed A. Alsharedah [a,*], Jonathan A. Black [b], Timothy Newson [c], M.H. El Naggar [c]

[a] Department of Civil Engineering, College of Engineering, Qassim University, Buraydah, 51452, Qassim, Saudi Arabia
[b] Department of Civil Engineering, School of Natural and Built Environment, Queen University of Belfast, Northern Ireland, United Kingdom
[c] Department of Civil & Environmental Engineering, College of Engineering, Western University, Canada

The authors regret the affiliation of the corresponding author. It was written as "[1]Department of Civil Engineering, Qassim University, Qassim, Saudi Arabia" and the authors would like to change it to "[1]Department of Civil Engineering, College of Engineering, Qassim University, Buraydah 51452, Qassim, Saudi Arabia."

Also, the reference Yu et al. (2019) is available in the text but missing in the references list and we would like to add it.

Hao Yu, Xiangwu Zeng, Bo Li, Jijian Lian, Centrifuge modeling of offshore wind foundations under earthquake loading, Soil Dynamics and Earthquake Engineering, Volume 77,2015, Pages 402–415, ISSN 0267–7261, https://doi.org/10.1016/j.soildyn.2015.06.014."

The affiliation change is requested by the first author institution.

The authors would like to apologise for any inconvenience caused.

References

Yu, H., Zeng, X., Li, B., Lian, J., 2015. Centrifuge modeling of offshore wind foundations under earthquake loading. Soil Dynam. Earthq. Eng. 77, 402–415. https://doi.org/10.1016/j.soildyn.2015.06.014. ISSN 0267–7261.

DOI of original article: https://doi.org/10.1016/j.oceaneng.2023.115421.

* Corresponding author.

E-mail addresses: y.alsharredah@qu.edu.sa (Y.A. Alsharedah), j.black@qub.ac.uk (J.A. Black), tnewson@eng.uwo.ca (T. Newson), naggar@uwo.ca (M.H. El Naggar).

https://doi.org/10.1016/j.oceaneng.2023.116583

Available online 21 December 2023